UNIVERSITY OF KENTUCKY
UKnowledge

**University of Kentucky**
**UKnowledge**

Physics and Astronomy Faculty Publications

Physics and Astronomy

12-27-2012

# Testing Diagnostics of Nuclear Activity and Star Formation in Galaxies at $z > 1$

Jonathan R. Trump
*University of California - Santa Cruz*

Nicholas P. Konidaris
*California Institute of Technology*

Guillermo Barro
*University of California - Santa Cruz*

David C. Koo
*University of California - Santa Cruz*

Dale D. Kocevski
*University of Kentucky*, dale.kocevski@uky.edu

*See next page for additional authors*

**Right click to open a feedback form in a new tab to let us know how this document benefits you.**

Follow this and additional works at: https://uknowledge.uky.edu/physastron_facpub

Part of the Astrophysics and Astronomy Commons, and the Physics Commons

**Authors**

Jonathan R. Trump, Nicholas P. Konidaris, Guillermo Barro, David C. Koo, Dale D. Kocevski, Stéphanie Juneau, Benjamin J. Weiner, S. M. Faber, Ian S. McLean, Renbin Yan, Pablo G. Pérez-González, and Victor Villar

**Testing Diagnostics of Nuclear Activity and Star Formation in Galaxies at $z > 1$**

# TESTING DIAGNOSTICS OF NUCLEAR ACTIVITY AND STAR FORMATION IN GALAXIES AT $z > 1$[*]

JONATHAN R. TRUMP[1], NICHOLAS P. KONIDARIS[2], GUILLERMO BARRO[1], DAVID C. KOO[1], DALE D. KOCEVSKI[3],
STÉPHANIE JUNEAU[4], BENJAMIN J. WEINER[5], S. M. FABER[1], IAN S. MCLEAN[6],
RENBIN YAN[3], PABLO G. PÉREZ-GONZÁLEZ[7], AND VICTOR VILLAR[7]

[1] University of California Observatories/Lick Observatory and Department of Astronomy and Astrophysics, University of California, Santa Cruz, CA 95064, USA
[2] Cahill Center for Astronomy and Astrophysics, California Institute of Technology, MC 105-24, 1200 East California Boulevard, Pasadena, CA 91125, USA
[3] Department of Physics and Astronomy, University of Kentucky, Lexington, KY 40506, USA
[4] Irfu/Service d'Astrophysique, CEA-Saclay, Orme des Merisiers, F-91191 Gif-sur-Yvette Cedex, France
[5] Steward Observatory, University of Arizona, 933 North Cherry Avenue, Tucson, AZ 85721, USA
[6] Department of Physics and Astronomy, UCLA, Los Angeles, CA 90095, USA
[7] Departamento de Astrofísica, Facultad de CC. Físicas, Universidad Complutense de Madrid, E-28040 Madrid, Spain

## ABSTRACT

We present some of the first science data with the new Keck/MOSFIRE instrument to test the effectiveness of different AGN/SF diagnostics at $z \sim 1.5$. MOSFIRE spectra were obtained in three *H*-band multi-slit masks in the GOODS-S field, resulting in 2 hr exposures of 36 emission-line galaxies. We compare X-ray data with the traditional emission-line ratio diagnostics and the alternative mass-excitation and color-excitation diagrams, combining new MOSFIRE infrared data with previous *HST*/WFC3 infrared spectra (from the 3D-HST survey) and multiwavelength photometry. We demonstrate that a high [O III]/H$\beta$ ratio is insufficient as an active galactic nucleus (AGN) indicator at $z > 1$. For the four X-ray-detected galaxies, the classic diagnostics ([O III]/H$\beta$ versus [N II]/H$\alpha$ and [S II]/H$\alpha$) remain consistent with X-ray AGN/SF classification. The X-ray data also suggest that "composite" galaxies (with intermediate AGN/SF classification) host bona fide AGNs. Nearly $\sim 2/3$ of the $z \sim 1.5$ emission-line galaxies have nuclear activity detected by either X-rays or the classic diagnostics. Compared to the X-ray and line ratio classifications, the mass-excitation method remains effective at $z > 1$, but we show that the color-excitation method requires a new calibration to successfully identify AGNs at these redshifts.

*Key words:* galaxies: active – galaxies: fundamental parameters – galaxies: nuclei – galaxies: Seyfert

*Online-only material:* color figures

## 1. INTRODUCTION

Every massive nearby galaxy hosts a supermassive black hole (SMBH), and the mass of the SMBH correlates with the mass of the host galaxy bulge (Magorrian et al. 1998). Theoretical simulations suggest that this connection exists because past active galactic nucleus (AGN) phases of rapid SMBH growth were associated with periods of massive star formation (SF) in the host galaxy (e.g., Di Matteo et al. 2005; Hopkins et al. 2008). Observations of AGN frequency, including both weak Seyferts and powerful quasars, in different host galaxy types over the cosmic time can be used to directly test models of coupled SMBH–galaxy growth.

Selection by blue optical color, X-ray emission, or infrared (IR) color can be used to select powerful quasars to very high redshifts, but these methods are less effective for finding obscured or moderately accreting AGNs. Instead the most efficient way to find moderate-luminosity AGNs is by their unique emission line signature. Compared to typical SF processes, the higher-ionization radiation of an AGN tends to increase the ratios between rest-frame optical collisionally excited "forbidden" lines and hydrogen recombination lines (Baldwin et al. 1981; Kewley et al. 2006). In particular the line ratios $f([\text{O III}]\,\lambda 5007)/f(\text{H}\beta)$, $f([\text{N II}]\,\lambda 6584)/f(\text{H}\alpha)$, and

$f([\text{S II}]\,\lambda 6718 + 6731)/f(\text{H}\alpha)$ are typically used in the classic "BPT" and "VO87" diagnostics (Baldwin et al. 1981; Veilleux & Osterbrock 1987): the wavelength proximity of each line pair means the ratios are nearly insensitive to reddening. In the standard AGN unified model (Antonucci et al. 1993), these narrow emission lines can be detected even if the X-ray and ultraviolet (UV) ionizing radiation source is absorbed by anisotropic obscuration. The AGN line ratio signature also remains visible for SMBHs of moderately low accretion rates ($L/L_{\text{Edd}} \sim 10^{-3}$) which are otherwise dominated by their host galaxy starlight (e.g., Kauffmann & Heckman 2009).

There has been great success in using line ratio diagnostics to select AGNs and characterize their hosts at $z \sim 0$ (e.g., Kauffmann et al. 2003a; Heckman et al. 2004; Yan et al. 2006; Schawinski et al. 2007). But extending a similar AGN census to $z > 0.4$ is difficult because the [N II]/H$\alpha$ and [S II]/H$\alpha$ ratios redshift to the IR, where ground-based spectroscopy has historically been expensive. A high [O III]/H$\beta$ ratio alone is degenerate between nuclear activity and metal-poor [H II] regions, and the [N II]/H$\alpha$ or [S II]/H$\alpha$ line ratio is generally necessary to distinguish AGNs from inactive galaxies with low metallicity. Some authors have suggested combining [O III]/H$\beta$ with bluer emission line ratios, like [O II] $\lambda 3726 + 3729$/H$\beta$ (Lamareille et al. 2004) or [Ne III] $\lambda 3869$/[O II] (Trouille et al. 2011). However, these bluer lines are typically weaker, making them difficult to apply to distant galaxies. Instead it is possible to exploit the correlation of metallicity with color and stellar mass (Tremonti et al. 2004) to altogether eliminate a second line ratio. These modified AGN/SF diagnostics use [O III]/H$\beta$ to measure excitation, but replace the [N II]/H$\alpha$ ratio with

rest-frame color (Yan et al. 2011) or stellar mass (Juneau et al. 2011). AGN selection using the "color-excitation (CEx)" and "mass-excitation (MEx)" methods agrees well with the classic line ratio diagnostics at $z < 0.4$ and X-ray selection at $z < 1$.

It is less clear if the BPT, VO87, CEx, and MEx AGN/SF diagnostics are directly applicable to higher redshift. SF processes at $z > 1$ are generally different than in nearby galaxies, with higher gas and dust fractions, younger stellar populations, lower metallicities, and higher star formation rates (SFRs; e.g., Papovich et al. 2005; Reddy et al. 2006; Tacconi et al. 2009; Shim et al. 2011). Some authors argue that the classical line ratio diagrams are unreliable at high redshift because local starburst galaxies with SF rates typical of $z > 1$ galaxies tend to have similarly high [N II]/H$\alpha$ and [O III]/H$\beta$ ratios (Liu et al. 2008; Brinchmann et al. 2008).

In this work, we directly test the effectiveness of the classical line ratio, color-excitation, and mass-excitation diagnostics for identifying AGNs at $z \sim 1.5$. We use observations of 36 galaxies at $1.30 < z < 1.62$ (mean $\bar{z} = 1.52$) with the new MOSFIRE multi-object spectrograph (McLean et al. 2010, 2012) on the Keck telescope. The new MOSFIRE data are coupled to X-ray observations, previous spectroscopy, and multiwavelength photometry for stellar masses and rest-frame colors.

## 2. OBSERVATIONAL DATA

We study the emission line ratios, rest-frame colors, stellar masses, and X-ray properties of 36 galaxies in the Great Observatories Origins Deep Survey-South field (GOODS-S; Giavalisco et al. 2004). The targets were selected from *Hubble Space Telescope* (*HST*) Wide Field Camera 3 (WFC3) G141 grism observations as part of the 3D-HST survey (Brammer et al. 2012). The initial selection required $F140W < 24$ and a detected [O III] emission line in the redshift range $1.3 < z < 1.7$. The flux-limited sample includes a mix of star-forming, AGN, and composite galaxies. New Keck/MOSFIRE *H*-band spectra were obtained for the [N II]/H$\alpha$ and [S II]/H$\alpha$ line ratios. The GOODS-S field also includes tremendously deep optical and IR photometry (Dahlen et al. 2010) and 4 Ms of X-ray coverage (Xue et al. 2011). Details on the WFC3 grism, MOSFIRE, and photometric data are provided below. Table 1 includes the full suite of line ratios, colors, and masses for the 36 galaxies. ACS *viz* color-composite images of eight representative galaxies are shown in Figure 1. In general the sample includes disk dominated and clumpy morphologies without strong point sources, similar to the clumpy galaxies and AGN hosts of Bournaud et al. (2012).

### 2.1. Keck/MOSFIRE

MOSFIRE observations were performed on 2012 September 14–15 and October 10, with three *H*-band masks in the GOODS-S field. All targets were observed in two dither positions within $0\farcs7$ slits, with total on-target exposure times of 2 hr each. The resulting wavelength coverage is $1.46 < \lambda < 1.81 \mu$m with a spectral resolution of $R \sim 3200$ ($\sim 5$ Å per resolution element). Spectra were reduced, sky subtracted, wavelength calibrated, and one-dimensional extracted using the public MOSFIRE data reduction pipeline.[8] Redshifts were found using the Specpro[9] software (Masters & Capak 2011). The wavelength calibration was very accurate, with shifts of $\Delta z \lesssim 0.001$ from previous

spectroscopic redshifts. The spectra were not flux calibrated: flux calibration is unnecessary for ratios of closely separated emission lines.

Figure 2 shows the sensitivity of MOSFIRE, for both emission lines and continuum measurements, in our 2 hr exposures. The left panel shows the emission-line signal-to-noise ratio (S/N) with line flux and SFR, using the Kennicutt (1998) relation to convert line flux at $z = 1.5$ to SFR. The right panel shows the continuum S/N (measured over a resolution element of 5 pixels) with F140W magnitude from 3D-HST observations. Continuum S/N is translated to the minimum rest-frame equivalent width (EW$_0$) for a $3\sigma$ line detection at $z = 1.5$, and F140W magnitude is converted to stellar mass using the relation $\log(M_*) = 21.3 - 0.5 m_{\mathrm{F140W}}$ (derived using the stellar masses from spectral energy distribution, SED, fitting in Section 2.3). In general, our sensitivity measurements agree well with the estimates provided on the MOSFIRE Web site.[10]

### 2.2. HST/WFC3 G141 Slitless Grism

The GOODS-S field contains publicly available *HST*/WFC3 G141 grism spectra to two-orbit depth as part of the 3D-HST survey (Brammer et al. 2012). We reduced the data using the aXe software (Kümmel et al. 2009; available at http://axe.stsci.edu/axe/), producing two-dimensional and one-dimensional wavelength- and flux-calibrated spectra with a wavelength range of $1.1 < \lambda < 1.7 \mu$m. The grism resolution is $R \simeq 130$ for a point source (46.5 Å pixel$^{-1}$) and somewhat worse for our extended galaxies. Spectra were inspected to identify contamination by neighboring objects: all of the objects studied here have H$\beta$ and [O III] emission lines unaffected by contamination.

### 2.3. Ancillary Photometry

The GOODS-S field has well-sampled SEDs from UV to IR wavelengths (Dahlen et al. 2010). The deep photometry, with high-confidence spectroscopic redshifts from MOSFIRE, allows for robust estimates of rest-frame colors and stellar masses for $z = 1.5$ galaxies. These quantities are computed following the methods of the Rainbow database[11] (Barro et al. 2011). First, the observed photometry is transformed to the rest frame using the spectroscopic redshift. The rest-frame SED is then fitted to a grid of Bruzual & Charlot (2003) models characterized by exponentially declining star formation histories, a Chabrier (2003) initial mass function, and a Calzetti (2001) extinction law. Stellar mass and rest-frame photometry are measured from the best-fit template. The well-sampled SED guarantees that the rest-frame $U-B$ color is interpolated rather than extrapolated.

The GOODS-S field also contains the deepest X-ray data in the sky, with 4 Ms of *Chandra* observations (Xue et al. 2011). Of the 36 galaxies in this study, 4 are X-ray detected: 3 of these are hard sources with $L_{2-8\,\mathrm{keV}} > 10^{42}$ erg s$^{-1}$ and are classified as AGNs by Xue et al. (2011), while 1 has soft X-ray emission consistent with SF. While the $L_x$/SFR relation indicates that SFR $> 1000\,M_\odot$ yr$^{-1}$ can also produce $L_{2-8\,\mathrm{keV}} > 10^{42}$ erg s$^{-1}$ (Lehmer et al. 2010; Mineo et al. 2012), such SFRs represent the extreme upper end of our sample (Figure 2). Indeed, all three of the sources classified as AGNs have X-ray luminosities at least 1.5 dex higher than expected by their H$\alpha$-derived SFRs. The X-ray sources are marked in Table 1, and we use the three X-ray AGNs as "truth" for testing the line ratio AGN/SF diagnostics in Section 4.

---

**Table 1**
Galaxy Properties

| ID | R.A. (deg) | Decl. (J2000) | $z$ | $f_{\rm [O\,III]}/f_{\rm H\beta}$ [a] | $f_{\rm [N\,II]}/f_{\rm H\alpha}$ [b] | $f_{\rm [S\,II]}/f_{\rm H\alpha}$ [b] | $\log(M_*)$ [c] $(\log(M_\odot))$ | $(U-B)_{\rm rest}$ [c] (mag) |
|---|---|---|---|---|---|---|---|---|
| 8025 | 53.07059 | −27.75539 | 1.303 | 0.45 | <0.24 | 1.65 | 10.40 | 0.88 |
| 6837 | 53.12799 | −27.77140 | 1.306 | >5.82 | 0.57 | 0.80 | 10.45 | 0.79 |
| 9956 | 53.09090 | −27.73119 | 1.307 | >5.61 | <0.33 | <0.58 | 9.09 | 0.57 |
| 6408 | 53.13639 | −27.77499 | 1.308 | 1.16 | <0.22 | 0.50 | 9.34 | 0.58 |
| 11132 | 53.08729 | −27.71850 | 1.308 | 1.43 | 0.24 | 0.19 | 9.64 | 0.79 |
| 8263 | 53.02619 | −27.75230 | 1.327 | 1.47 | <0.45 | 0.60 | 9.80 | 0.63 |
| 11404[d] | 53.12480 | −27.71710 | 1.356 | 2.12 | 0.28 | 0.33 | 10.80 | 0.80 |
| 11730 | 53.14540 | −27.71260 | 1.361 | 4.10 | <0.38 | 0.73 | 9.26 | 0.62 |
| 9038[e] | 53.07529 | −27.74259 | 1.374 | 1.80 | 0.26 | 0.24 | 10.02 | 0.53 |
| 7835 | 53.05199 | −27.75839 | 1.376 | >2.77 | <0.19 | 0.22 | 10.46 | 0.70 |
| 10123 | 53.12810 | −27.72929 | 1.426 | 5.77 | 0.23 | 0.21 | 9.25 | 0.47 |
| 11010 | 53.05690 | −27.72030 | 1.473 | 1.56 | 0.14 | 0.18 | 9.93 | 0.44 |
| 7042 | 53.06560 | −27.76790 | 1.539 | 2.57 | 0.44 | 0.17 | 10.36 | 0.81 |
| 9915 | 53.13259 | −27.73229 | 1.549 | 1.28 | 0.48 | 0.29 | 10.57 | 1.03 |
| 11349 | 53.10960 | −27.71719 | 1.552 | 5.79 | 0.18 | 0.76 | 9.12 | 0.29 |
| 12961 | 53.09719 | −27.69860 | 1.576 | 1.18 | <0.08 | <0.12 | 10.12 | 0.76 |
| 5745 | 53.07379 | −27.78420 | 1.607 | 2.46 | 0.09 | <0.13 | 9.52 | 0.33 |
| 11993 | 53.11220 | −27.71100 | 1.608 | 3.01 | 0.31 | 0.27 | 10.52 | 0.74 |
| 13252 | 53.09469 | −27.69459 | 1.608 | 5.47 | 0.25 | 0.23 | 10.30 | 0.68 |
| 10366 | 53.07300 | −27.72680 | 1.608 | 4.97 | 0.15 | <0.18 | 9.65 | 0.62 |
| 8753 | 53.10430 | −27.74650 | 1.609 | 2.82 | 0.41 | 0.37 | 10.54 | 0.83 |
| 10917 | 53.10910 | −27.72150 | 1.610 | 6.36 | 0.06 | 0.14 | 9.72 | 0.41 |
| 6842 | 53.07300 | −27.77050 | 1.610 | 1.76 | 0.29 | 0.16 | 10.38 | 0.73 |
| 12278 | 53.16040 | −27.70770 | 1.610 | 1.35 | 0.34 | <0.36 | 10.43 | 0.73 |
| 11534 | 53.12319 | −27.71559 | 1.610 | 3.49 | 0.30 | 0.20 | 10.41 | 0.79 |
| 9792 | 53.03450 | −27.73340 | 1.611 | 3.47 | <0.09 | <0.15 | 9.51 | 0.54 |
| 10817[e] | 53.12279 | −27.72279 | 1.612 | >7.49 | 1.03 | 0.27 | 10.70 | 0.84 |
| 8803 | 53.13290 | −27.74580 | 1.612 | 1.45 | 0.20 | 0.40 | 10.42 | 0.82 |
| 8154 | 53.14730 | −27.75349 | 1.612 | >3.20 | 0.36 | 0.40 | 10.45 | 0.76 |
| 7371 | 53.08409 | −27.76370 | 1.612 | 2.17 | 0.11 | 0.12 | 9.58 | 0.36 |
| 12285 | 53.11000 | −27.70789 | 1.613 | 5.47 | 0.14 | 0.18 | 10.52 | 0.71 |
| 7989 | 53.10279 | −27.75609 | 1.613 | 4.74 | 0.45 | <0.10 | 10.06 | 0.66 |
| 12703 | 53.11370 | −27.70149 | 1.613 | 4.03 | 0.27 | 0.21 | 11.11 | 0.90 |
| 12522[e] | 53.10490 | −27.70520 | 1.613 | 2.83 | 0.52 | 0.22 | 10.84 | 0.64 |
| 8414 | 53.15650 | −27.75079 | 1.614 | 0.88 | <0.21 | 0.46 | 9.33 | 0.39 |
| 7499 | 53.14110 | −27.76189 | 1.622 | 0.68 | 0.36 | 0.40 | 10.08 | 0.79 |

**Notes.**
[a] The $f_{\rm [O\,III]}$ and $f_{\rm H\beta}$ line flux measurements come from the WFC3 grism data.
[b] The $f_{\rm H\alpha}$, $f_{\rm [N\,II]}$, and $f_{\rm [S\,II]}$ emission line fluxes are measured from the MOSFIRE data.
[c] Stellar mass and rest-frame color are estimated from SED fitting, as described in Section 2.3.
[d] X-ray detected and classified as an AGN by Xue et al. (2011).
[e] X-ray detected, but in the soft band only and consistent with emission from a star-forming galaxy (Xue et al. 2011).

## 3. AGN/SF DIAGNOSTICS

We compare the classical line ratio with the color-excitation and mass-excitation AGN/SF diagnostics, using emission line ratios measured from the spectra and photometry-derived rest-frame colors and stellar masses. The MOSFIRE $H$-band spectra provide [N II], [S II], and Hα fluxes, while Hβ and [O III] are measured from the WFC3 grism spectra. Examples of the emission-line fitting are shown in Figure 3.

For the high-resolution MOSFIRE spectra, a continuum is fit across the emission line regions by splining the 50 pixel smoothed continuum. The emission line intensities are then computed simply as the sum of the continuum-subtracted flux in each of the wavelength regions $6556 < \lambda < 6570$ (Hα), $6578 < \lambda < 6592$ ([N II]), and $6711 < \lambda < 6740$ (both [S II] lines).

Line flux measurements in the low-resolution WFC3 grism spectra are more difficult because the Hβ and [O III] lines are blended. For the grism spectra, we subtract a linear continuum over the wavelength region $4750 < \lambda < 5120$ and then fit three Gaussians, each of which are restricted to be within 20 Å ($\sim$1200 km s$^{-1}$) of the line centers (4861 Å, 4959 Å, and 5007 Å). The [O III] λ5007 flux is computed as 3/4 of the sum of the blended [O III] Gaussians (Storey & Zeippen 2000).

Errors in line fluxes and ratios are calculated by bootstrapping 10,000 realizations of the resampled data. These errors accurately quantify the difficulty in line fitting when there is significant contamination by sky lines in MOSFIRE or nearby objects in the WFC3 grism. We use $1\sigma$ upper limits for undetected emission lines.

Figure 4 presents the color-excitation and mass-excitation diagrams along with the traditional BPT ([O III]/Hβ versus [N II]/Hα and [O III]/Hβ versus [S II]/Hα) AGN/SF diagnostics for the $z \sim 1.5$ galaxies. The solid lines give the AGN/SF separation line defined for each diagram (CEx: Yan et al. 2011; MEx: Juneau et al. 2011; BPT and VO87: Kewley
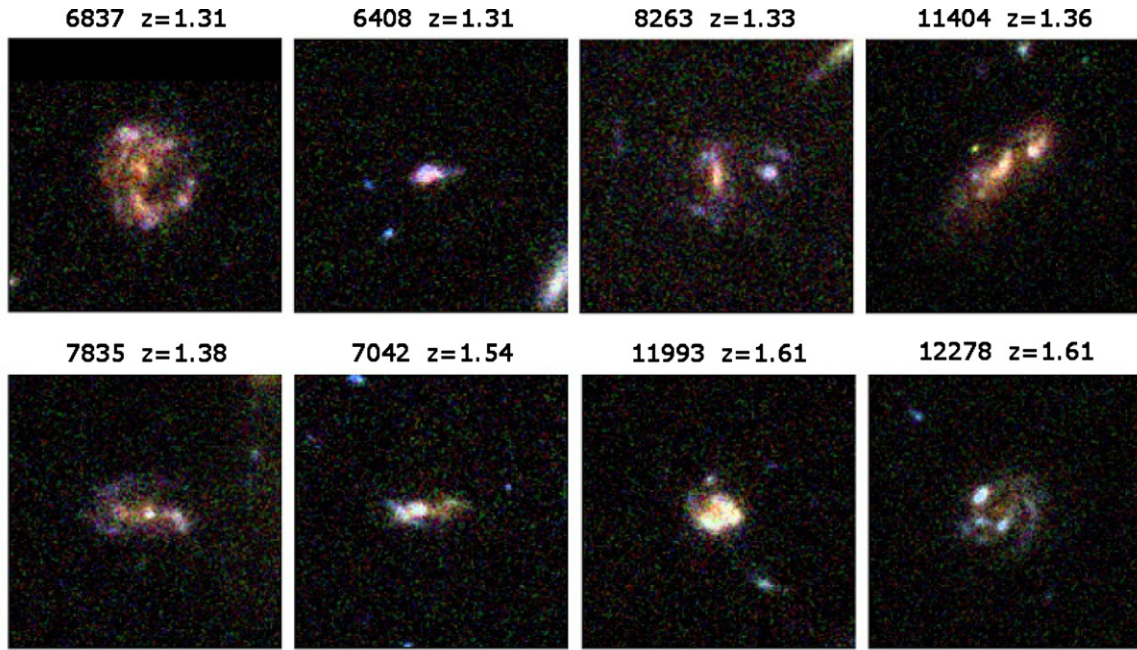
**Figure 1.** ACS *viz* color-composite $5'' \times 5''$ images for 8 of the 36 emission-line galaxies, selected to be representative of the full sample's range in redshift, stellar mass, and AGN/SF classification. At $z \sim 1.5$ these thumbnails span $42 \times 42$ kpc. Galaxy No. 11404 (upper right panel) is an X-ray AGN. The rest-frame UV images of the full set of 36 galaxies (including those shown here) exhibit a range of disk dominated and clumpy morphologies without strong point sources.

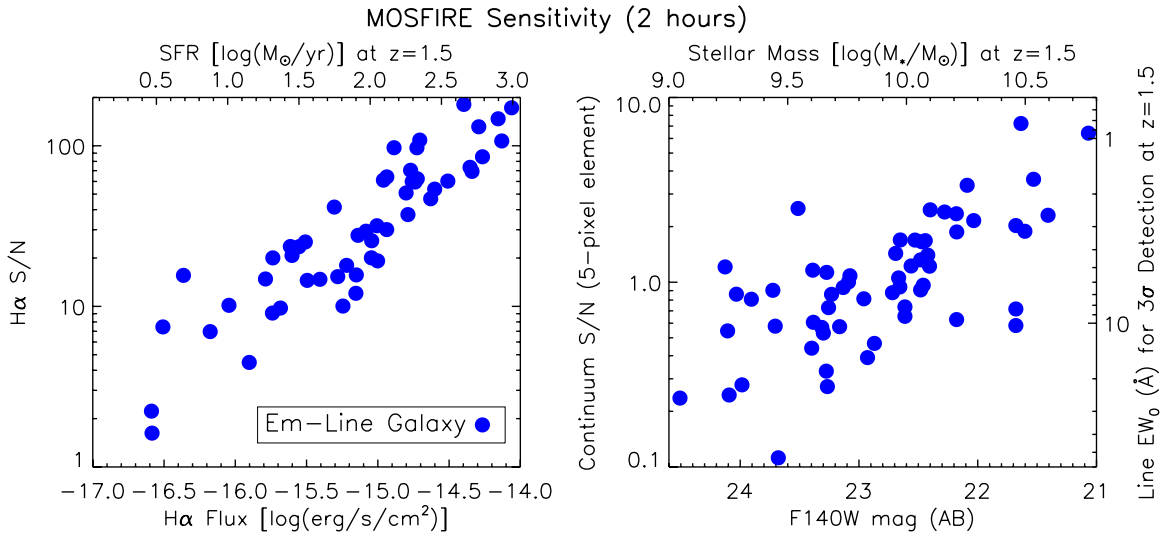(A color version of this figure is available in the online journal.)



**Figure 2.** Sensitivity of MOSFIRE to emission lines and continuum measurements for 2 hr exposures. At left is shown the measured S/N and flux for $H\alpha$ in our targets, with the upper axis translating these line fluxes to SFR (using the Kennicutt 1998 relation at $z = 1.5$ with a standard $\Lambda$CDM cosmology and $h_0 = 0.7$). Note that the SFR axis is inaccurate for galaxies with significant AGN contribution to their $H\alpha$ flux. The right panel shows the continuum signal-to-noise ratio (per 5 pixel resolution element) and corresponding rest-frame EW limit for $3\sigma$ line detection vs. $F140W$ magnitude and corresponding stellar mass, using the empirical relation $\log(M_*) = 21.3 - 0.5 m_{F140W}$.

(A color version of this figure is available in the online journal.)

et al. 2006), with AGNs having $\log([O\,\textsc{iii}]/H\beta)$ above this line and star-forming galaxies lying below. Each panel also includes a comparison sample of $z < 0.3$ galaxies from the Sloan Digital Sky Survey (SDSS; York et al. 2000) MPA-JHU value-added DR7 catalog.[12] These $z < 0.3$ galaxies have emission line and stellar mass measurements described by Tremonti et al. (2004) and Kauffmann et al. (2003b), with rest-frame magnitudes calculated using the kcorrect IDL software (Blanton & Roweis

2007). The $z \sim 1.5$ galaxies are color-coded according to their Kewley et al. (2006) AGN/SF classification as follows.

1. *X-ray sources*: filled red circles for AGNs and filled blue diamonds for galaxies (as classified by Xue et al. 2011).
2. *SF galaxy, blue crosses*: $\log([O\,\textsc{iii}]/H\beta) < 1.3 + 0.61/[\log([N\,\textsc{ii}]/H\alpha) - 0.05]$.
3. *Composite SF+AGN, open green diamonds*: $\log([O\,\textsc{iii}]/H\beta) > 1.3+0.61/[\log([N\,\textsc{ii}]/H\alpha)-0.05]$ and $\log([O\,\textsc{iii}]/H\beta) < 1.19+0.61/[\log([N\,\textsc{ii}]/H\alpha)-0.47]$, from Kauffmann et al. (2003a).
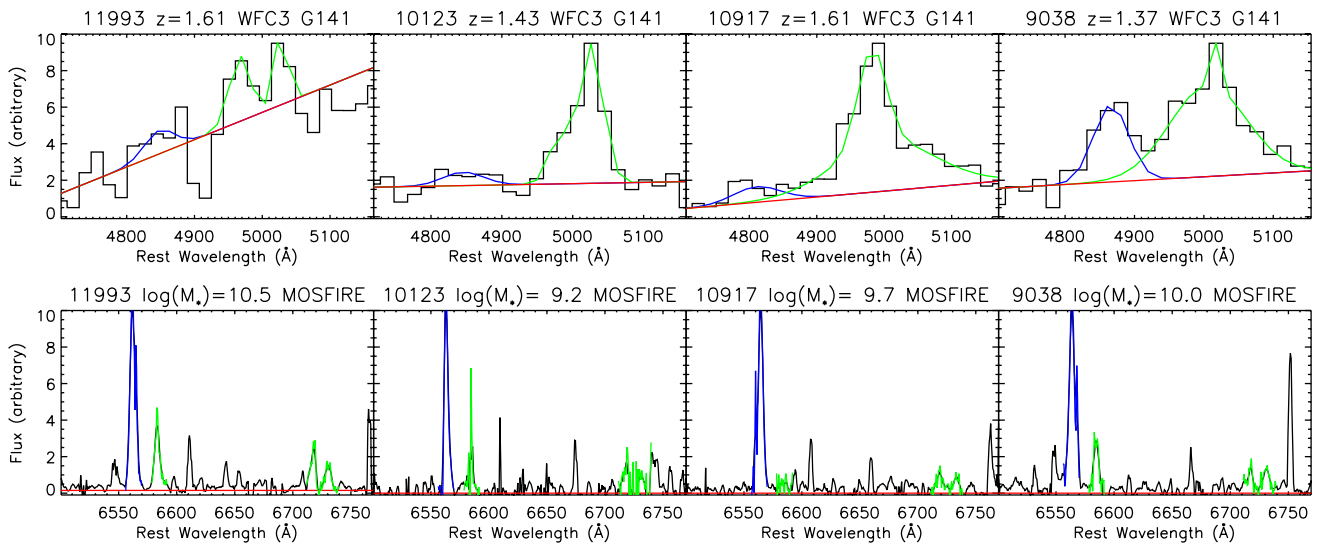
---

[12] http://www.mpa-garching.mpg.de/SDSS/

**Figure 3.** Examples of emission-line fit to the WFC3 grism and MOSFIRE spectra. The black histogram shows the spectrum, with the continuum fit in red and the emission line regions in blue (Hα and Hβ) and green ([O III], [N II], and [S II]). In the high-resolution MOSFIRE data, the (uncalibrated) line intensity is computed by simply summing the continuum-subtracted spectrum in the line region. However, the Hβ and [O III] emission lines overlap in the low-resolution WFC3 grism data, and the line flux is instead calculated from Gaussians fitted to the continuum-subtracted spectrum. The object in the rightmost panels (ID No. 9038) is X-ray detected, but has both emission line and X-ray properties of a star-forming galaxy.

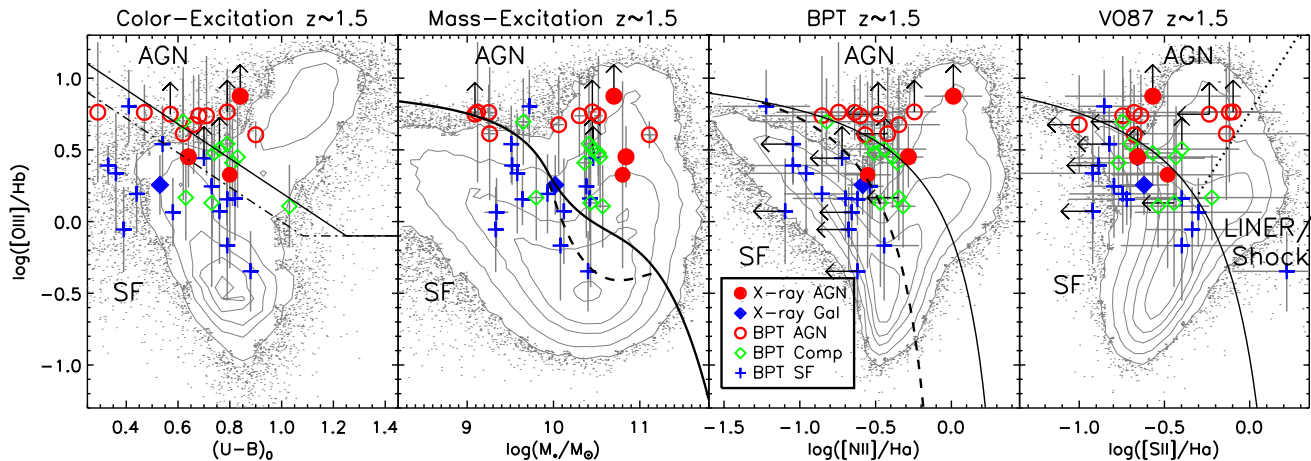(A color version of this figure is available in the online journal.)



**Figure 4.** AGN/SF diagnostics: from left to right, color-excitation with [O III]/Hβ flux ratio vs. rest-frame $U-B$ color (Yan et al. 2011), mass-excitation with [O III]/Hβ vs. stellar mass (Juneau et al. 2011), the [O III]/Hβ vs. [N II]/Hα BPT diagram, and the [O III]/Hβ vs. [S II]/Hα VO87 diagram. The Hβ and [O III] emission lines are measured from the WFC3 grism, while the Hα, [N II], and [S II] lines are measured from the new MOSFIRE data. AGNs sit in the upper right of each panel, while star-forming galaxies (dominated by [H II] regions) sit below and to the left of the solid lines. The dashed lines of the MEx and BPT diagrams display the "composite" regions of both nuclear activity and star formation, and the dotted line in the [S II]/Hα panel separates Seyfert AGNs from LINERs. Galaxies are color-coded based on their X-ray and Kewley et al. (2006) classifications. In contrast to $z < 0.3$ galaxies (gray contours), most of the $z \sim 1.5$ galaxies have properties near the AGN/SF dividing line of each diagnostic method. At $z \sim 1.5$, the MEx method remains consistent with the BPT diagnostics, but the CEx method misses several AGNs identified by the other methods. The dot-dashed line in the CEx diagram shows our revised AGN/SF demarcation (see Section 4).

(A color version of this figure is available in the online journal.)

4. *AGN, open red circles*: $\log([O III]/H\beta) > 1.19 + 0.61/[\log([N II]/H\alpha) - 0.47]$ and $\log([O III]/H\beta) > 0.76 + 1.89 \log([S II]/H\alpha)$.

5. *LINER/Shock*: $\log([O III]/H\beta) > 1.19 + 0.61/[\log([N II]/H\alpha) - 0.47]$ and $\log([O III]/H\beta) < 0.76 + 1.89 \log([S II]/H\alpha)$.

None of the $z \sim 1.5$ galaxies meet the LINER/Shock criteria, although the elevated [S II]/Hα ratios of several $z \sim 1.5$ galaxies classified as star forming (by their [N II]/Hα and [O III]/Hβ ratios) support the conclusion of Yan & Blanton (2012) that such systems are excited by shocks rather than AGN ionization.

Galaxies at $z \sim 1.5$ have typically higher [O III]/Hβ ratios than $z < 0.3$ galaxies, in agreement with previous $z > 1$ studies (e.g., Liu et al. 2008; Wright et al. 2010; Trump et al. 2011).

However, this is not necessarily because $z \sim 1.5$ galaxies are more likely to be AGNs: low-metallicity star-forming galaxies (in the upper left of each panel in Figure 4) are also more likely at $z > 1$. An elevated [O III]/Hβ ratio is insufficient for AGN identification at $z > 1$.

## 4. AGN IDENTIFICATION AT $z > 1$

Determining the effectiveness of each AGN/SF diagnostic requires knowledge of the "true" AGN population. The X-ray data provide an independent AGN/SF classification method. For the four X-ray-detected galaxies, the X-ray classifications of Xue et al. (2011) generally agree with the Kewley et al. (2006) classifications: the three X-ray AGNs have emission line

ratios indicative of either AGNs or composite AGN+SF systems, while the X-ray galaxy has star-forming emission-line ratios. The classic AGN/SF line ratio classifications remain accurate for the four X-ray-detected galaxies at $z \sim 1.5$.

The X-ray detection of galaxies in or near the "composite" region, with line ratios intermediate between AGN and SF, implies that these objects do in fact host accreting AGNs. These data are in contrast with Liu et al. (2008) and Brinchmann et al. (2008), who argued that AGN/SF composite galaxies at $z > 1$ are starbursts with unusual gas properties and no significant AGNs. Galaxies in the composite region may host starbursts, but the X-ray data imply that they also host genuine AGNs. Indeed, many studies suggest a connection between SF activity and AGN accretion (e.g., Kauffmann et al. 2003a; Trump et al. 2012). The analyses of Wright et al. (2010) and Trump et al. (2011), with spatially resolved emission line ratio gradients, provide additional evidence that $z > 1$ AGN/SF composite galaxies host nuclear activity.

The lack of an X-ray detection in the other 32 galaxies does not mean that they lack AGNs. X-ray surveys are less sensitive to moderate-luminosity AGNs in galaxies of lower stellar masses (Aird et al. 2012), and all three X-ray-detected AGNs have the highest stellar masses in our sample ($\log(M_*/M_\odot) > 10.7$). X-ray surveys are also insensitive to heavily obscured AGNs. Because the Kewley et al. (2006) classifications match the X-ray data for the high-mass X-ray-detected galaxies, we conclude that these classifications are robust for $z > 1$ galaxies. Of the 32 X-ray undetected galaxies, those identified as AGNs by their line ratios are presumably undetected because they have low stellar masses or are X-ray obscured.

The total number of AGNs from the combined X-ray and line ratio classifications is 11/36, with an additional 10/36 AGN/SF composite galaxies. Thus, about 1/3 of our $z > 1$ emission-line galaxies are AGN dominated, and nearly $\sim 2/3$ have some AGN component. This is significantly higher than the $\sim 15\%$ AGNs and composite fraction at $z \sim 0$ (Kauffmann et al. 2003a), although this may be partly driven by our emission-line selection.

The mass-excitation method remains generally consistent with the BPT/VO87 and X-ray classifications at $z \sim 1.5$. Juneau et al. (2011) emphasize that a probabilistic approach is more meaningful with the MEx method than simply classifying individual galaxies by the AGN/SF dividing line. Following Juneau et al. (2011), the MEx probability analysis indicates that $\sim 18/36$ galaxies are AGNs, matching the high AGN fraction of the X-ray and BPT/VO87 classifications.

Meanwhile, the color-excitation method, as calibrated at $z \sim 0$, identifies only 7 of the 12 AGNs classified by X-rays or line ratios. This is because a $z \sim 1.5$ galaxy has significantly higher SFR and lower metallicity and is consequently bluer than a $z \sim 0$ galaxy of the same mass (Erb et al. 2006; Mannucci et al. 2010). While the change in metallicity is apparent in the increasing [O III]/H$\beta$ ratio, the change in SFR is not. Shifting the original AGN/SF division of Yan et al. (2011) by 0.2 mag provides a much more effective separation between AGNs from SF galaxies at $z \sim 1.5$. Our data suggest the following recalibrated color-excitation AGN/SF demarcation at $z > 1$:

$$\log([\text{O III}]/\text{H}\beta) = \max[1.2 - 1.2(U - B)_0, -0.1].$$

## 5. SUMMARY

We use some of the first Keck/MOSFIRE data to test various diagnostics of AGN/SF activity in 36 emission-line galaxies at $z \sim 1.5$. Although only four sources are X-ray detected, their X-ray data suggest that the classic emission-line ratio diagnostic remains effective at $z > 1$, and that "composite" galaxies (of intermediate AGN/SF classification) do in fact host accreting AGNs. We find that nearly $\sim 2/3$ of our $z \sim 1.5$ emission-line galaxies have some AGN contribution detected by X-rays or line ratios. Among alternative AGN/SF diagnostics, the mass-excitation method remains consistent with X-ray and line ratio classification at $z \sim 1.5$, but the color-excitation method does not. We suggest a recalibration for AGN/SF classification with the color-excitation diagnostic at $z > 1$. A larger set of galaxies and emission line measurements will allow a more detailed calibration and estimation of the AGN fraction at $z > 1$.

## REFERENCES

Aird, J., Coil, A. L., Moustakas, J., et al. 2012, ApJ, 746, 90
Antonucci, R. 1993, ARA&A, 31, 473
Baldwin, J. A., Phillips, M. M., & Terlevich, R. 1981, PASP, 93, 5
Barro, G., Perez-Gonzalez, P. G., Gallego, J., et al. 2011, ApJS, 193, 30
Blanton, M. R., & Roweis, S. 2007, AJ, 133, 734
Bournaud, F., Juneau, S., Le Floc'h, E., et al. 2012, ApJ, 757, 81
Brammer, G. B., van Dokkum, P. G., Franx, M., et al. 2012, ApJS, 200, 13
Brinchmann, J., Pettini, M., & Charlot, S. 2008, MNRAS, 385, 769
Bruzual, G., & Charlot, S. 2003, MNRAS, 344, 1000
Calzetti, D. 2001, PASP, 113, 1449
Chabrier, G. 2003, PASP, 115, 763
Dahlen, T., Mobasher, B., Dickinson, M., et al. 2010, ApJ, 724, 425
Di Matteo, T., Springel, V., & Hernquist, L. 2005, Natur, 433, 604
Erb, D. K., Shapley, A. E., Pettini, M., et al. 2006, ApJ, 644, 813
Giavalisco, M., Ferguson, H. C., Koekemoer, A. M., et al. 2004, ApJ, 600, 93
Heckman, T. M., Kauffmann, G., Brinchmann, J., et al. 2004, ApJ, 613, 1
Hopkins, P. F., Hernquist, L., Cox, T. J., et al. 2008, ApJS, 175, 356
Juneau, S., Dickinson, M., Alexander, D. M., & Salim, S. 2011, ApJ, 736, 104
Kauffmann, G., & Heckman, T. M. 2009, MNRAS, 397, 135
Kauffmann, G., Heckman, T. M., Tremonti, C., et al. 2003a, MNRAS, 346, 1055
Kauffmann, G., Heckman, T. M., White, S. D. M., et al. 2003b, MNRAS, 341, 33
Kennicutt, R. C., Jr. 1998, ARA&A, 36, 189
Kewley, L. J., Groves, B., Kauffmann, G., & Heckman, T. 2006, MNRAS, 372, 961
Kümmel, M., Walsh, J. R., Pirzkal, N., Kuntschner, H., & Pasquali, A. 2009, PASP, 121, 59
Lamareille, F., Mouhcine, M., Contini, T., Lewis, I., & Maddox, S. 2004, MNRAS, 350, 396
Lehmer, B. D., Alexander, D. M., Bauer, F. E., et al. 2010, ApJ, 724, 559
Liu, X., Shapley, A. E., Coil, A. L., Brinchmann, J., & Ma, C.-P. 2008, ApJ, 678, 758
Magorrian, J., Tremaine, S., Richstone, D., et al. 1998, AJ, 115, 2285
Mannucci, F., Cresci, G., Maiolino, R., Marconi, A., & Gnerucci, A. 2010, MNRAS, 408, 2115
Masters, D., & Capak, P. 2011, PASP, 123, 638
McLean, I. S., Ramsay, S. K., & Takami, H. 2010, Proc. SPIE, 7735, 47
McLean, I. S., Steidel, C. C., Epps, H. W., et al. 2012, Proc. SPIE, 8446, 84460

Mineo, S., Gilfanov, M., & Sunyaev, R. 2012, MNRAS, submitted (arXiv:1207.2157)
Papovich, C., Dickinson, M., Giavalisco, M., Conselice, C. J., & Ferguson, H. C. 2005, ApJ, 631, 101
Reddy, N. A., Steidel, C. C., Fadda, D., et al. 2006, ApJ, 644, 792
Schawinski, K., Thomas, D., Sarzi, M., et al. 2007, MNRAS, 382, 1415
Shim, H., Chary, R.-R., Dickinson, M., et al. 2011, ApJ, 738, 69
Storey, P. J., & Zeippen, C. J. 2000, MNRAS, 312, 813
Tacconi, L. J., Genzel, R., Neri, R., et al. 2009, Natur, 463, 781
Tremonti, C. A., Heckman, T. M., Kauffmann, G., et al. 2004, ApJ, 613, 898

Trouille, L., Barger, A. J., & Tremonti, C. 2011, ApJ, 742, 46
Trump, J. R., Weiner, B. J., Scarlata, C., et al. 2011, ApJ, 743, 144
Trump, J. R., Hsu, A. D., Fang, J. J., et al. 2012, ApJ, in press (arXiv:1212.0544)
Veilleux, S., & Osterbrock, D. E. 1987, ApJS, 63, 295
Wright, S. A., Larkin, J. E., Graham, J. R., & Ma, C.-P. 2010, ApJ, 711, 1291
Xue, Y. Q., Luo, B., Brandt, W. N., et al. 2011, ApJS, 195, 10
Yan, R., & Blanton, M. R. 2012, ApJ, 747, 61
Yan, R., Ho, L. C., Newman, J. A., et al. 2011, ApJ, 728, 38
Yan, R., Newman, J. A., Faber, S. M., et al. 2006, ApJ, 648, 281
York, D. G., Adelman, J., Anderson, J. E., Jr., et al. 2000, AJ, 120, 1579